

# A Single Residue in the S6 Transmembrane Domain Governs the Differential Flecainide Sensitivity of Voltage-gated Potassium Channels

DANIEL HERRERA, AIDA MAMARBACHI, MANUEL SIMOES, LUCIE PARENT, RÉMY SAUVÉ, ZHIGUO WANG, and STANLEY NATTEL

*From the Research Center and Department of Medicine (D.H., A.M., Z.W., S.N.), Montreal Heart Institute and University of Montreal; Departments of Pharmacology (D.H.) and Physiology (M.S., L.P., R.S.), University of Montreal; Department of Pharmacology and Therapeutics, (S.N.), McGill University, Montreal, Quebec, Canada.*

This work was supported by the Canadian Institutes of Health Research, the Quebec Heart and Stroke Foundation and the Mathematics of Information Technology and Complex Systems (MITACS) Network.

**Running title:** S6 Domain Residue and Kv Blocker Sensitivity

**Correspondence to:** Dr Stanley Nattel, Research Center, Montreal Heart Institute,  
5000 Belanger St E, Montreal, Quebec, Canada, H1T 1C8. Tel.: (514)-376-3330;  
Fax: (514)-376-1355; E-mail: stanley.nattel@icm-mhi.org

**Number of text pages:** 17

**Number of tables:** 3

**Number of figures:** 8

**Number of references:** 47

**Number of words in the Abstract:** 225

**Number of words in the Introduction:** 362

**Number of words in the Discussion:** 1839

**Abbreviations:**

HERG = human ether-a-go-go-related gene

$I_{K_{ur}}$  = ultrarapid-delayed rectifier currents

KcsA = streptomyces lividans potassium channel

Kv = voltage-gated  $K^+$

MthK = methanobacterium thermoautotrophicum potassium channel

PCRs = polymerase chain reactions

$V_{1/2}$  = half-maximal activation voltage

WT = wild-type

## ABSTRACT

Flecainide has been used to differentiate Kv4.2-based transient-outward K<sup>+</sup>-currents (flecainide-sensitive) from Kv1.4-based (flecainide-insensitive). We found that flecainide also inhibits ultrarapid-delayed rectifier (I<sub>Kur</sub>) currents in *Xenopus* oocytes carried by Kv3.1 subunits (IC<sub>50</sub>, 28.3±1.3 μM) more strongly than Kv1.5 currents corresponding to human I<sub>Kur</sub> (237.1±6.2 μM). The present study examined molecular motifs underlying differential flecainide sensitivity. An initial chimeric approach pointed to a role for S6 and/or carboxy-terminal sites in Kv3.1/Kv1.5 sensitivity-differences. We then looked for homologous amino-acid residues of the two sensitive subunits (Kv4.2 and Kv3.1) different from homologous residues for insensitive subunits (Kv1.4 and Kv1.5). Three candidate sites were identified: two in the S5-S6 linker and one in the S6 segment. Mutation of the proximal S5-S6 linker site failed to alter flecainide-sensitivity. Mutation at the more distal site in Kv1.5 (V481L) modestly increased sensitivity, but the reciprocal Kv3.1 mutation (L401V) had no effect. S6 mutants caused marked changes: flecainide sensitivity decreased ~8-fold for Kv3.1 L422I (to IC<sub>50</sub> 213±9 μM) and increased ~7-fold for Kv1.5 I502L (to 35.6±1.9 μM). Corresponding mutations reversed flecainide-sensitivity of Kv1.4 and Kv4.2: L392I decreased Kv4.2-sensitivity ~17-fold (from IC<sub>50</sub> 37.4±6.9 to 628±36 μM); I547L increased Kv1.4-sensitivity ~15-fold (from 706±37 to 40.9±7.3 μM). Our observations indicate that the flecainide sensitivity differences among these four voltage-gated K<sup>+</sup>-channels are determined by whether an isoleucine or a leucine is present at a specific amino acid location.

## Introduction

Voltage-gated  $K^+$ -channels of the Shaker family play an important role in governing cardiac excitability (Roden and George 1997; Snyders, 1999). A variety of antiarrhythmic agents target Shaker-based channels (Tamargo et al., 2004; Varro et al., 2004), and such actions are believed to contribute to their actions in man. The cardiac transient outward current ( $I_{to}$ ) subunits Kv1.4 and Kv4.2 differ in their sensitivity to the antiarrhythmic drug flecainide, with Kv4.2 being much more sensitive than Kv1.4. This difference has been used to probe the various contributions of Kv1.4 and Kv4.2 to native  $I_{to}$  in the rat (Yeola and Snyders, 1997). Kv1.5, the principal ionic current underlying human atrial ultra-rapid delayed rectifier current ( $I_{Kur}$ ) (Wang et al., 1993; Feng et al., 1997) is a potentially interesting atrial-selective ionic target for drug therapy of atrial fibrillation (AF) (Nattel et al., 1999). The dog counterpart,  $I_{Kur,d}$ , appears to have a contribution from Kv3.1 subunits (Yue et al., 1996; Yue et al., 2000a), although the importance of this contribution has recently been questioned (Fedida et al., 2003). In previous work, we found  $I_{Kur,d}$  to be sensitive to flecainide (Yue et al., 2000b), unlike human  $I_{Kur}$ , which appears resistant (Wang et al., 1995). In preliminary studies, we observed corresponding differences in the flecainide sensitivity of Kv3.1 and Kv1.5 (Herrera et al., 2002), reminiscent of the differences typically observed between Kv4.2 and Kv1.4. The present study was designed to characterize flecainide block of Kv3.1 and Kv1.5, and then to determine whether there is a common molecular basis for flecainide-sensitivity differences between Kv1.4 and Kv1.5 on one hand, and Kv3.1 and Kv4.2 on the other.

We began by constructing several chimeras of the Kv3.1 and Kv1.5 wild-type channels to identify important domains of flecainide block in these channels. This was followed by site-directed mutagenesis of the identified domains to determine whether specific residues might

modulate sensitivity of these channels to flecainide. The results of these studies pointed to a key role for the presence of leucine versus isoleucine at a specific amino acid location. Finally, a mathematical model was applied to assess the location and orientation of this amino acid in relation to key structures in the Kv3.1 channel molecule.

## Materials and Methods

**Molecular Biology.** Wild-type (WT) dKv3.1 (GenBank #AF153198), hKv1.5 (GenBank #XM\_006988, kindly provided by Dr. Barbara Wible) and rKv1.4 (GenBank #NM\_012971, kindly provided by Dr. Barbara Wible), were cloned into a pSP64 (Promega, Madison, WI) and rKv4.2 (GenBank #S64320, kindly provided by Dr. Jeanne Nerbonne) into a pRC-CMV expression vector (Invitrogen Life Technologies, Carlsbad, CA) with identical restriction endonuclease sites flanking the clone in the polyclonal region for ligating the digest product into the target vector.

For chimera construction we performed a series of polymerase chain reactions (PCRs) with Elongase Enzyme Mix (Invitrogen Life Technologies) and respective WTs as templates. For overlap extension of both products we used a third PCR and the products of each of the previous reactions as the template. The synthetic oligonucleotide primers used for the first reactions contained the ends of the chimera and the restriction endonuclease sites for cloning into the expression vector (Table 1). The complementary primer contained part of one clone and an overlap overhang for the overlap extension PCR. The third PCR employed the end primers to create a continuous string of nucleotides of the desired sequence. The final products and target vectors were digested with appropriate restriction endonucleases (Table 1) and ligated with Quick T4 DNA ligase (New England Biolabs, Beverley, MA).

For site-directed mutagenesis, PCR was applied, with a synthetic oligonucleotide primer containing the desired nucleotide to create the point mutation upon translation. Two complementary primers containing desired mutation and PCR primers flanking unique restriction enzyme sites enclosed the region of interest. Two parallel PCR reactions, each with a flanking primer and a primer containing the desired mutation, generated two DNA fragments with

overlapping ends. After gel purification, both fragments were annealed in a third PCR using the two restriction site flanking primers, resulting in a fragment containing the desired mutation. The final PCR product was digested with the flanking restriction enzymes, gel-purified, and TOPO-TA cloned into the PCRII vector. All PCR-generated sequences were verified by double-stranded sequencing. After sequence confirmation, the mutant was released from PCRII at flanking restriction sites and ligated into pSP64 (or pRC-CMV) containing the coding region for the respective WT from which the segments enclosed by the restriction enzyme sites had been removed.

**Oocyte Isolation.** Frogs were anesthetized by immersion in tricaine methanesulfonate for approximately 25 minutes. Oocytes were excised and immersed in a 100-mm Petri dish containing Barth's solution (mM): 100 NaCl, 2.0 KCl, 1.8 CaCl<sub>2</sub>, 1.0 MgCl<sub>2</sub>, and 5.0 HEPES, pH 7.4 (NaOH) at room temperature. Oocytes were physically separated, then immersed (~60 minutes) in 7 ml of calcium-free Barth's-collagenase solution containing (mM): 82.5 NaCl, 2.0 KCl, 1.0 MgCl<sub>2</sub>, and 5.0 HEPES, 0.0247 g lyophilized collagenase type A (Invitrogen) and 0.0075 g trypsin inhibitor. Oocytes were incubated in Barth's solution containing penicillin (1000 U/L) (Invitrogen), streptomycin (100 mg/L) (Invitrogen), kanamycin (100 mg/L) and sodium pyruvate (275 mg/L) (Sigma) for 12 hours at 15°C.

5'-Capped polyadenylated cRNA was prepared for each construct with the SP6 mMessage mMachine in-vitro transcription kit (Ambion) after cDNA linearization. *Xenopus* oocytes were injected with ~1-1.4 ng/oocyte of cRNA using a microinjector and stored for at least 12 hours in Barth's solution containing antibiotics and 5% horse serum at 15°C. Oocytes were placed in a recording/perfusion chamber and perfused at 0.5 mL/min with (mM): 5.0 KCl, 100 NaCl,

2.0 MgCl<sub>2</sub>, 0.3 CaCl<sub>2</sub>, 10 *N*-2-hydroxyethylpiperazine-*N'*-2-ethanesulfonic acid (HEPES), pH 7.4 (NaOH).

**Data Acquisition and Analysis.** Whole-cell currents were recorded at room temperature with 2-electrode voltage-clamp. Borosilicate-glass electrodes (outer diameter 1.0 mm) filled with 3 M KCl (resistances 1-2 M $\Omega$ ) were connected to a GeneClamp-500B amplifier (Axon). Current-injecting electrode resistance averaged 1.5 M $\Omega$ . Voltage command pulses were generated with pClamp 6 software connected to a 12-bit Digidata 1200 analog-to-digital converter (Axon). A holding potential (HP) of -60 mV was used as in previous studies of native currents (Yue et al., 2000; Wang et al., 1995). The effects of flecainide (Sigma) exposure were monitored with test pulses to +60 mV (in 10 mV steps). The inter-pulse interval was 10 seconds for all protocols and pulse length is indicated in figure insets. Recordings were low-pass filtered at 1 kHz. Data were analyzed with pClamp 6 (Axon Instruments) and are expressed as mean $\pm$ S.E.M. Group comparisons were performed with ANOVA. If significant differences were indicated by ANOVA, a *t*-test with Bonferroni's correction was used to evaluate differences between individual mean values. A two-tailed *P*<0.05 was taken to indicate statistical significance.

**Homology Modeling of the Kv3.1 Pore.** Two models of the Kv3.1 channel were generated using the KcsA (*Streptomyces lividans*) potassium channel (PDB: 1J95) and the MthK (*Methanobacterium thermoautotrophicum*) potassium channel (PDB: 1LNQ) channel structures as templates. The sequence alignment between the Kv3.1 pore-S6 region, MthK and KcsA was performed with SAM-T02 (Hughey and Krogh, 1996). Automated homology modeling was

carried out with Modeller V6.2 (Sali and Blundell, 1993) and involved the generation of 150 models of the Kv3.1 channel pore for each structural template. Model selection was based on the lowest objective function value (roughly related to the energy of the model) provided by Modeller (Sali and Blundell, 1993) and on the RMS deviation between the atomic coordinates of the template relative to the model. Energy minimization was carried out on the four best models using Charmm (Brooks et al., 1983). The overall structural quality of the generated models was confirmed by PROCHECK (Laskowski et al., 1993). Structural features of flecainide were approximated using HyperChem 7.5 (Hyperchem, Gainesville, FL) and the AMBER force field (Weiner et al., 1984).

## Results

**Effects of Flecaïnide on Kv3.1 and Kv1.5.** The effects of flecaïnide on Kv3.1 WT and Kv1.5 WT were characterized by eliciting currents in response to pulses to potentials ranging from -50 to +60 mV in increments of 10 mV from a holding potential of -60 mV. Test pulses elicited rapidly activating outward currents with very slow inactivation in the absence of flecaïnide (Fig. 1). Reduced current increments were seen for Kv3.1 at potentials positive to +30 mV, compatible with inward rectification, as previously described for dKv3.1 (Yue et al., 1996; Yue et al., 2000a). Flecaïnide (50  $\mu$ M) caused rapid decay of Kv3.1 currents upon depolarization, compatible with open-channel block, and potently decreased end-pulse current amplitude (Fig. 1A). Overall, 50  $\mu$ M flecaïnide significantly inhibited dKv3.1 current at all voltages positive to 0 mV, with a mean  $58.9 \pm 3.9\%$  reduction at +30 mV (Fig. 1B). In contrast, the same concentration of flecaïnide had little apparent effect on Kv1.5 currents (Fig. 1C), and mean Kv1.5 current amplitude was not significantly affected (Fig. 1D). These observations indicate important differences between Kv1.5 and Kv3.1 in their sensitivity to the drug.

Figure 2 shows the effects of the full range of drug concentrations on Kv3.1 and Kv1.5. Figure 2A illustrates the effects of increasing drug concentrations on current recorded upon stepping from -60 to +30 mV in single oocytes expressing each subunit. Flecaïnide appreciably decreased Kv3.1 current at 20  $\mu$ M and produced near-total block of end-pulse current at 500  $\mu$ M. In contrast, Kv1.5 was minimally affected by 50  $\mu$ M flecaïnide and 500  $\mu$ M drug produced just over 50% inhibition. Figure 2B shows mean concentration-response data for flecaïnide inhibition of Kv3.1 and Kv1.5 at +30 mV. The flecaïnide  $IC_{50}$ s for Kv3.1 end-pulse current at +30 mV averaged  $28.3 \pm 1.3$   $\mu$ M with a Hill coefficient ( $n_H$ ) of  $0.91 \pm 0.1$  in 11 oocytes, an order of magnitude less than the corresponding value for Kv1.5 ( $237.1 \pm 6.2$   $\mu$ M, Hill coefficient  $1.1 \pm 0.2$

$n=8$  oocytes,  $P<0.001$ ). Figure 2C shows the percentage inhibition by two concentrations of flecainide on Kv3.1 and Kv1.5 at different test potentials. Inhibition showed shallow voltage-dependence for both subunits. At approximately equipotent flecainide concentrations (50  $\mu\text{M}$  for Kv3.1, 500  $\mu\text{M}$  for Kv1.5), block as a function of voltage is not significantly different for the two subunits. Figures 2D and 2E show the activation curve for Kv3.1 and Kv1.5, respectively, based on an analysis of tail currents following 400-ms test pulses to various activation voltages, before and after exposure to approximately equipotent drug concentrations. The half-maximal activation voltage ( $V_{1/2}$ ) of Kv3.1 was  $-1.7\pm 0.4$  mV (slope factor  $8.2\pm 1.3$  mV), and this was slightly shifted to  $-6.8\pm 1.5$  mV, ( $P<0.05$ ; slope factor  $7.4\pm 1.9$  mV) after exposure to flecainide. For Kv1.5, the  $V_{1/2}$  was  $-11.6\pm 1.8$  mV (slope factor  $7.2\pm 1.8$  mV) before and  $-16.9\pm 1.9$  mV (slope factor  $7.4\pm 1.9$  mV) after 500  $\mu\text{M}$  flecainide.

The rapid decay of current in the presence of flecainide suggests open-channel blocking. Figure 3A (inset) shows the onset of Kv3.1 block as a function of time during the pulse at three concentrations of flecainide. Block was a discrete function of time, well-fit by exponential relations as shown, and accelerated at higher drug concentrations. The regression lines in Fig 3A are an analysis of blocking kinetics as a function of drug concentration. The blocking rate constant ( $K$ ) was a linear function of concentration ( $C$ ), consistent with a standard blocking model,  $K = k_{\text{off}} + k_{\text{on}}[C]$  (where  $k_{\text{off}}$  and  $k_{\text{on}}$  are rate constants for drug-receptor association and dissociation).  $K$  is obtained from best-fit regression of the onset of block at each concentration to a single exponential function  $B(t) = B_o + B_{\text{id}}(1 - \exp[-Kt])$ , where  $B(t)$  is block at time  $t$ ,  $B_o$  = block upon pulse onset and  $B_{\text{id}}$  = steady-state time-dependent block. The dissociation constant ( $K_d$ ) is given by  $k_{\text{off}}/k_{\text{on}}$  and the exponential block-onset time constant  $\tau_B$  at any concentration  $[C]$  is given by  $1/(k_{\text{on}}[C] + k_{\text{off}})$ , with the net rate constant  $K$  being  $1/\tau_B$ . When this relation was

analyzed in each of 8 experiments with Kv3.1, we obtained a mean  $k_{\text{on}}$  of  $1.4 \pm 0.1 \mu\text{M}^{-1}\text{s}^{-1}$  and  $k_{\text{off}}$  of  $39.8 \pm 5.3 \text{ s}^{-1}$ . The  $K_{\text{d}}$  estimated from  $k_{\text{off}}/k_{\text{on}}$  of the kinetic analysis averaged  $28.8 \pm 3.6 \mu\text{M}$ , in good agreement with the directly measured  $\text{IC}_{50}$  ( $28.3 \mu\text{M}$ ) as obtained in Fig. 2A. Figure 3B shows corresponding data for Kv1.5. The results are qualitatively similar, with lower blocking rates for a given concentration. For Kv1.5,  $k_{\text{on}}$  averaged  $0.30 \pm 0.02 \mu\text{M}^{-1}\text{s}^{-1}$  and  $k_{\text{off}}$   $60.0 \pm 5.5 \text{ s}^{-1}$  ( $n=8$  oocytes).  $K_{\text{d}}$  estimated from the kinetic analysis averaged  $210.8 \pm 5.9 \mu\text{M}$ , once again in reasonable agreement with the directly measured  $\text{IC}_{50}$  ( $237 \mu\text{M}$ ). Table 2 shows the calculated rate constants. The time-dependent block onset in Fig. 3A and B are compatible with open-channel block. This notion is further supported by observations of crossover of control tail currents with those in the presence of blocking drug concentrations for Kv3.1 (Fig. 3C) and Kv1.5 (Fig. 3D). Upon repolarisation in the absence of drug, rapid time-dependent transition of channels from the open to the closed state provides characteristic deactivating tail currents. In the presence of drug, deactivation of unblocked channels is similarly rapid. However, for many open-channel blockers, unblocking must occur in the open state, there is low affinity for the closed state and drug-bound channels must unblock before closing. If a large fraction of channels have been blocked during depolarization and the unbinding rate  $k_{\text{off}}$  is fast enough, channels may unblock through the open state upon repolarization and carry significant current, thus slowing the apparent rate of deactivation. This process will be reflected in a slower time course of the tail current, resulting in tail current 'crossover' (Armstrong, 1971). The tail-current time course was fitted by monoexponential relations (as shown by the solid lines fitted to the experimental data points shown in Figures 3C and D), providing the mean data shown in Figure 3E. These results show that the rate of current decay upon repolarisation was prolonged significantly in the presence of drug. Kv3.1 tail-current time constants increased from  $54.8 \pm 2.7 \text{ ms}$  (control) to

218.2±9.6 ms in presence of flecainide 50 μM ( $P=0.0017$ ,  $n=8$  oocytes). Corresponding values for Kv1.5 before and after 100 μM flecainide were 115.6±3.0 ms and 247.4±7.2 ms, respectively ( $P=0.0173$ ,  $n=8$  oocytes).

**Response of Kv3.1/Kv1.5 Chimeras to Flecainide.** As an initial approach to analyzing the molecular determinants of the differential flecainide sensitivity of Kv3.1 and Kv1.5, we constructed chimeras between the two subunits. Two sets of reciprocal chimeras were constructed. Since we had already observed block of the wild-type channels in their open configuration we decided to concentrate on the pore to C-terminal region (see figure 3C, D and E). One set of chimeras involved the C-terminal distal to position Asn-436 in Kv3.1 and Asn-518 in Kv1.5. Figure 4A, top panels, show typical recordings before and after 50 μM flecainide in WT Kv3.1 and Kv1.5, whereas the middle panels show corresponding recordings from Kv3.1 subunits with their C-terminal replaced by those of Kv1.5 and Kv1.5 subunits with Kv3.1 C-terminal substitution. There was clearly no major change in sensitivity. We therefore interchanged longer segments of each subunit, involving the C-terminal distal to Met-414 in the Kv3.1 S6 segment and Lys-494 in the Kv1.5 S6. Figure 4A (bottom panels) show that flecainide sensitivity was somewhat decreased for Kv3.1 subunits containing the S6+C-terminal component of Kv1.5 and that sensitivity was increased for the corresponding Kv1.5 chimera. Figure 4B compares mean±S.E.M. concentration-response data for the S6+C-terminal chimeras with those of WTs at +30 mV. Results for the chimeras clearly lie in a position different from those of the WTs and close to each other. Mean  $IC_{50s}$  at +30 mV based on values calculated for each oocyte studied for WT and both sets of chimeric constructs are shown in Fig. 4C. Whereas values for the C-terminal chimeras are indistinguishable from WT, values for the S6+C-terminal chimeras

are significantly different from their respective WTs and not different from each other. These results suggest that molecular motifs in S6 play a role in determining the flecainide affinity differences between Kv3.1 and Kv1.5. We next proceeded to address the potential role of specific amino acid residues in these drug affinity differences.

**Effects of Mutating Candidate Amino Acids in Kv3.1 and Kv1.5 on Flecainide Sensitivity.** The results described above suggest that flecainide produces open-channel block of both Kv3.1 and Kv1.5, with marked differences in affinity. We noted that similar differences in flecainide affinity had previously been reported for Kv1.4 (Yamagishi et al., 1995), which like its Kv1 subfamily co-member Kv1.5 is flecainide-insensitive, and Kv4.2 (Caballero et al., 2003), which is typically flecainide-sensitive. In addition, we noted that many of the amino acids that determine drug block of voltage-dependent K<sup>+</sup>-channels are situated in the S5-S6 linker region or in S6 (Yeola et al., 1996; Franqueza et al., 1997; Zhang et al., 1998; Caballero et al., 2002; Decher et al., 2004). We therefore aligned and compared these portions of the sequences of rKv1.4, hKv1.5, dKv3.1 and rKv4.2 with one another. As shown in Fig. 5, there was a large degree of homology among these subunits. At three positions (shown by boxes and symbols corresponding to their respective position in the channel protein), amino-acid residues corresponded for Kv1.4 and Kv1.5, on one hand, and for Kv3.1 and Kv4.2, on the other, but differed between the sensitive and insensitive subunits.

We therefore considered these three amino acid residues to be candidates to play a role in the difference in flecainide sensitivity between the sensitive subunits Kv3.1 and Kv4.2 and the insensitive subunits Kv1.4 and Kv1.5. We first used site-directed mutagenesis to alter each of these amino acids in Kv3.1 to those in Kv1.5, and to alter the amino acids in Kv1.5 to those in Kv3.1. Figure 6A illustrates the effects of several flecainide concentrations on current at +30 mV

in oocytes expressing WT subunits and each of the point mutations. The response of Kv3.1 subunits with the I389D mutation was similar to that of the WT subunits shown immediately above. Similarly, Kv1.5 with the reciprocal D469I mutation responded like Kv1.5 WT. The response of L401V Kv3.1 also resembled that of Kv3.1 WT, but the reciprocal V481L Kv1.5 appeared somewhat more sensitive to flecainide than Kv1.5 WT. The mutations shown in the bottom panels of Fig. 6A had quite striking effects. The L422I mutation strongly decreased the sensitivity of Kv3.1, whereas I502L strongly increased that of Kv1.5.

Figure 6B shows the mean  $IC_{50}$ s for each of the constructs studied at +30 mV. The isoleucine/aspartic acid mutations did not alter the  $IC_{50}$  of either Kv3.1 or Kv1.5. Whereas Kv3.1 L401V had an  $IC_{50}$  indistinguishable from that of Kv3.1 WT, Kv1.5 V481L had a significantly lower  $IC_{50}$  than that of Kv1.5 WT. The most striking changes occurred with the isoleucine/leucine mutations in the S6 segment. The  $IC_{50}$  of Kv3.1 L422I was dramatically increased from that of Kv3.1 WT and approached the value of Kv1.5 WT. Similarly, the  $IC_{50}$  of Kv1.5 I502L was substantially decreased and approximated that of Kv3.1 WT. The full concentration-response relations for flecainide inhibition of the reciprocal isoleucine/leucine mutants and their respective WTs are shown in Fig. 6C. They indicate that the S6 isoleucine/leucine mutants transformed the flecainide-sensitivity phenotype of each subunit to resemble that of its opposite WT counterpart. Table 2 shows the rate constants for leucine/isoleucine mutants compared to WTs, and indicate that like the WT channels, the main differences among the mutants was in the  $k_{on}$ , suggesting that the differences in drug sensitivity were due to differences in drug access to the channel rather than stability of the drug-receptor complex.

**Biophysical Effects of the S6 Isoleucine/Leucine Mutations in Kv3.1 and Kv1.5.** To evaluate changes in biophysical properties as potential mechanisms of altered flecainide-sensitivity of the S6 Kv3.1 and Kv1.5 mutants, we assessed the kinetics, activation voltage-dependence and reversal potentials of the currents carried by the various constructs. As shown in Table 3, despite the substantial changes in flecainide-sensitivity caused by the mutations, they did not affect the primary biophysical properties of the channels.

**Effects of Corresponding Mutations in Kv1.4 and Kv4.2.** The striking changes in Kv3.1 and Kv1.5 flecainide sensitivity caused by the S6 isoleucine/leucine mutations suggest a crucial role in determining the flecainide sensitivity differences between these subunits. To determine the role of the corresponding residues in Kv1.4 and Kv4.2, we made the equivalent point mutations in these subunits. The results are illustrated in Fig. 7. Figure 7A (left panels) shows currents recorded upon voltage steps from -80 mV in Kv4.2 WT, Kv4.2 with the S6 L492I mutation, Kv1.4 WT and Kv1.4 I547L. The right panels show currents recorded from the same oocytes after exposure to 50  $\mu$ M flecainide. Kv4.2 WT was clearly flecainide-sensitive and Kv1.4 WT flecainide-insensitive. The leucine to isoleucine mutation at position 392 abolished the response to 50  $\mu$ M flecainide in Kv4.2, without obviously affecting current kinetics. On the other hand, the reciprocal mutation in Kv1.4 substantially increased flecainide sensitivity. Figure 7B shows the full concentration-response relations for the WT subunits and the isoleucine/leucine mutants at +30 mV. The mutations clearly reversed the flecainide-sensitivity differences, with curves for each point-mutated subunit superimposing on the curve of the opposite WT subunit. Overall, Kv4.2 WT exhibited marked sensitivity to flecainide with an  $IC_{50}$  of  $37.4 \pm 6.9 \mu$ M, compared to Kv1.4 WT which had an  $IC_{50}$  of  $706.3 \pm 37.2 \mu$ M ( $P < 0.001$  versus Kv4.2). The

Kv1.4 I547L mutant  $IC_{50}$  was decreased to  $40.9 \pm 7.3 \mu\text{M}$  ( $P < 0.001$  versus Kv1.4 WT), whereas the flecainide  $IC_{50}$  of the Kv4.2 L392I mutant was  $628.3 \pm 35.5 \mu\text{M}$  ( $P < 0.001$  versus Kv4.2 WT).

## Discussion

In this study, we have evaluated the basis for pharmacological sensitivity differences among four voltage-dependent  $K^+$ -channel subunit channels. We find that a single, relatively conservative amino acid difference in S6 accounts for the variations in flecainide sensitivity.

### Comparison with Previous Studies of Molecular Determinants of Cardiac Ion-Channel

**Block.** Replacing a leucine with an isoleucine in corresponding positions of the S6 transmembrane domain conferred to the flecainide-sensitive channels Kv3.1 and Kv4.2 a flecainide affinity like that of the insensitive subunits Kv1.4 and Kv1.5. Mutating the equivalent isoleucine in Kv1.4 and Kv1.5 to a leucine conferred strongly-increased sensitivity similar to that of Kv3.1 and Kv4.2. These subunits possess highly-conserved S5, pore and S6 segments.

Several previous studies have examined molecular motifs in these subunits that determine antiarrhythmic drug binding (Caballero et al, 2002; Decher et al, 2004; Franqueza et al, 1997; Yeola et al, 1996). Yeola et al. (1996) were the first to examine the determinants of quinidine binding in Kv1.5. They noted that residues in the S6 segment, specifically T507 and V514, are significant determinants of quinidine block. Franqueza et al. (1997) showed that mutations at T507, L510 and V514 abolish stereoselectivity of bupivacaine block of Kv1.5. Caballero et al. (2002) examined the determinants of benzocaine block and low-concentration agonist activity on Kv1.5, and found that mutations of T479, T507, L510 and V514 abolish agonist actions but increase blocking effects. In a recent study, Decher et al. (2004) used alanine-scanning mutagenesis to examine the role of 23 amino acids in the  $K^+$ -signature sequence and S6 of Kv1.5 in sensitivity to the anthranilic acid derivative S0100176. Mutations at T479, T480, V505, I508 and V512 reduced drug sensitivity. An alanine mutation at I502, the critical site in the present

study, slightly but significantly decreased sensitivity to S0100176. The authors concluded that specific S6 and pore helix residues facing the inner cavity form a binding pocket for S0100176. There is also evidence for a role of S6 residues in determining drug block of Kv1.4 channels. Substitutions at T529 alter sensitivity to quinidine and 4-aminopyridine (4AP), with a phenylalanine substitution in particular strongly reducing the affinity for quinidine (Zhang et al., 1998). Phenylalanine substitutions in the leucine heptad repeat region of the S4-S5 linker region stabilize the closed state of Kv1.4 and increase 4AP sensitivity (Judge et al., 2002).

There is evidence for an important role of S6 residues in governing drug block of other cardiac voltage-gated potassium channels. Mutations at S620 and S631 impair C-type inactivation of the rapid delayed-rectifier channel encoded by the *human ether-a-go-go-related gene* (HERG) and attenuate verapamil block (Zhang et al., 1999). Changes in HERG inactivation due to S6 mutations can be dissociated from alterations in blocking drug affinity, suggesting a primary role for modulation of drug affinity rather than state-dependent block (Lees-Miller et al., 2000). An elegant series of studies from Dr. Sanguinetti's laboratory have revealed the structural basis for HERG block, with cation- $\pi$  interactions involving critical S6 residues and tertiary nitrogens playing a central role (Mitcheson et al, 2000; Fernandez et al., 2004). Similarly, S6 domain residues are crucial determinants of drug block of the slow delayed-rectifier channel KvLQT1 (Seebahm et al., 2003), voltage-gated Na<sup>+</sup>-channels (Ragsdale et al., 1996; Sunami et al., 1997), and L-type Ca<sup>2+</sup>-channels (Hockerman et al., 1997).

**Model of Kv3.1 Channel Pore.** We used molecular modeling to evaluate the position of the critical leucine/isoleucine amino-acid residue in relation to key structural components of Kv3.1. The results of structural modeling (according to the approach described in the "Materials and

Methods” section) are shown in Fig. 8. The overall structure of the S5-pore-S6 region of Kv3.1 is illustrated in a ribbon representation, with the surface of the L422 and V425 residues colored in yellow and red respectively. The V425 residue is seen as projecting inside part of the channel central cavity (Jiang et al., 2002). This residue has been shown to participate in the binding of a large number of inhibitory agents to several K<sup>+</sup> channels, including the voltage-gated Shaker (Liu et al., 1997) and the KCa3.1 (Wulff et al., 2001) channels. As the dimensions of the channel inner cavity (10Å) correspond to the computed length of a flecainide molecule, it is quite conceivable that flecainide interacts directly with the hydrophobic residues of the channel cavity, in particular V425. In contrast, the van der Waals surface of the key L422 residue appears to be projecting directly behind V425. Hence, our structural analysis does not support a direct interaction between flecainide and the residue at position 422; therefore, it is probably not part of the binding site *per se*. It is possible, however, that the L to I mutation at position 422 induces a repositioning of the V425 residue, thereby modifying the interaction between flecainide and residues such as V425 in the channel cavity. Alternatively, as seen in the model in Figure 8, L422 is located directly above the highly-conserved G424 residue that is generally considered to act as a gating hinge. This residue bends the inner helix by approximately 30 degrees in the crystal structure of MthK and is believed to provide part of the S6 segment flexibility required for Kv channel opening. It is thus possible that the L422I mutation alters the flexibility of the G424 region, thus modulating the rate at which flecainide has access to the channel inner cavity.

Figure 8 also includes the position of the hydrophilic L401 (green) and I389 (blue) residues, mutation of which failed to alter flecainide sensitivity of Kv3.1. The I389 residue is predicted to be located in the N-terminal end of the channel pore helix (blue) whereas the L401 residue is seen as part of the selectivity filter. Because I389 is more exposed to the external than internal medium, mutating this residue is not expected to affect the structure of the channel central cavity.

However, according to the proposed model, the leucine at position 401 could indirectly modify the position of the cavity-lining T400 residue and thus affect flecainide binding. In fact, residues at positions equivalent to T400 have been implicated in drug binding (see for instance Wulff et al., 2001). However, mutation of L401 is not likely to result in a significant change in the T400 orientation due to the high rigidity of the filter region.

The predicted positions of the I389, L401, L422 and V425 residues depend on the validity of our homology-based models. In this regard, it should be pointed out that the structural features of the L401, L422 and V425 residues are conserved whether Kv3.1 is modeled with MthK (Figure 8) or with the closed KcsA channel structure as template (not shown). The structure of the S6 segment above the gating-hinge glycine residue thus appears to change minimally between the closed and the open conformation of K<sup>+</sup>-channels, despite important structural changes in the C-terminal region of S6. However, in the absence of a crystal structure for mammalian voltage-gated K<sup>+</sup> channels, we cannot rule out the possibility that the orientation of the L422 and V425 residues differs from that predicted by the bacterial MthK and/or KcsA structures. Further studies to evaluate the potential structural basis for the role of the isoleucine/leucine moiety in determining flecainide sensitivity, as well as the importance of other residues in that region, would be of interest.

**Potential Importance of our Findings.** The difference in flecainide-sensitivity between Kv1.4 and Kv4.2 is well-recognized and consequently flecainide has been used as a tool to explore the potential molecular basis of native I<sub>to</sub> (Yeola and Snyders, 1997; Han et al., 2000). Flecainide sensitivity differences have also been noted between canine I<sub>Kur</sub> with properties of Kv3.1 (Yue et al., 2000) and native human Kv1.5-like I<sub>Kur</sub> currents (Wang et al., 1995). The present study demonstrates a common molecular basis for these sensitivity differences: the

presence of a leucine rather than an isoleucine at a key S6 amino-acid position in the flecainide-sensitive subunits.

Atrial fibrillation is the most common clinical arrhythmia and its treatment remains suboptimal (Nattel et al., 2002). Because of its atrial-selective localization, Kv1.5-based human  $I_{Kur}$  has been suggested to be a potentially-interesting target for new antiarrhythmic drug development (Wang et al., 1993). The present study was designed to shed light on the molecular determinant of reported differences seen between sensitive and insensitive subunits. The identification of a key amino-acid determinant is an important step in this direction. A better understanding of the molecular determinants of the drug-sensitivity of Kv1.5 and related channels may help in the rational design of new antiarrhythmic compounds.

**Potential Limitations.** The objective of this study was to determine the molecular basis for the differences in flecainide sensitivity among four subunits involved in forming native  $K^+$ -channels for which discrepancies in sensitivity have been noted and studied previously. We did not set out to establish the details of the molecular determinants of the drug-binding site for each individual subunit. Although the latter issue is of great interest, it goes well beyond the scope of the present study. The S6+C-terminal chimeras containing the S6+C-terminal of Kv3.1 or Kv1.5 moved the flecainide sensitivity towards that of the subunit composition of the S6+C-terminal end. However, despite the fact that the S6+C-terminal contained the leucine/isoleucine moiety conferring flecainide sensitivity/insensitivity respectively in the respective wild types or point mutations, the changes in drug sensitivity were less with the chimeras than for the point mutations. This observation suggests that other molecular determinants in S6 and/or the C-terminus influence drug sensitivity in the chimeras, and can partly offset the effects of the leucine/isoleucine moiety.

The channel-blocking concentrations in this study are higher than those produced therapeutically, as well as values published in studies analyzing the effects of flecainide on  $I_{Kur,d}$  in isolated atrial cells and in vivo models of AF (Yue et al., 2000b; Wang et al., 1992). This discrepancy is likely due to the well-recognized lesser sensitivity to blocking drugs of channels expressed in *Xenopus* oocytes compared to mammalian cells (Weerapura et al, 2002). Nevertheless, the mechanisms of channel block in *Xenopus* oocytes are believed to be similar to those in other systems and *Xenopus* oocytes are widely used as an expression system for the analysis of structural motifs for channel block (Decher et al., 2004; Dibb et al., 2003; Perry et al., 2004; Wang et al., 2003).

We used molecular modeling to evaluate the position of the critical leucine/isoleucine amino acid in relationship to key structural components of Kv3.1. We recognize that this modeling does not clarify the details of flecainide binding. As mentioned above, a full evaluation of the molecular structure of the drug-binding site goes beyond the scope of this study. In particular, further work is needed to delineate the amino acids that form the binding site and the mechanism of their interaction with the critical leucine/isoleucine residue that we identified. Nevertheless, we feel that it is important to note the position of the leucine/isoleucine amino acid site in order to begin to assess potential mechanisms of its involvement. Further work will clearly be needed to reveal more of the details of flecainide's interactions with channels composed of Kv4.2, Kv3.1, Kv1.4 and Kv1.5 subunits.

### **Acknowledgments**

The authors thank Evelyn Landry and Xiaofan Yang for expert technical assistance and France Thériault for excellent secretarial help with the manuscript.

## References

- Armstrong CM (1971) Interaction of tetraethylammonium ion derivatives with the potassium channels of giant axons. *J Gen Physiol* **58**:413-437.
- Brooks BR, Bruccoleri RE, Olafson BD, States DJ, Swaminathan S, and Karplus M (1983) A Program for Macromolecular Energy Minimization and Dynamics Calculations. *J Comput Chem* **4**:187-217.
- Caballero R, Pourrier M, Schram G, Delpon E, Tamargo J, and Nattel S (2003) Effects of flecainide and quinidine on Kv4.2 currents: voltage dependence and role of S6 valines. *Br J Pharmacol* **138**: 1475-1484.
- Caballero R, Moreno I, Gonzalez T, Valenzuela C, Tamargo J, and Delpon E (2002) Putative binding sites for benzocaine on a human cardiac cloned channel (Kv1.5). *Cardiovasc Res* **56**:104-117.
- Decher N, Pirard B, Bundis F, Peukert S, Baringhaus KH, Busch AE, Steinmeyer K, and Sanguinetti MC (2004) Molecular basis for Kv1.5 channel block: conservation of drug binding sites among voltage-gated K<sup>+</sup> channels. *J Biol Chem* **279**:394-400.
- Dibb KM, Rose T, Makary SY, Claydon TW, Enkvetchakul D, Leach R, Nichols CG, and Boyett MR (2003) Molecular basis of ion selectivity, block, and rectification of the inward rectifier Kir3.1/Kir3.4 K<sup>+</sup> channel. *J Biol Chem* **278**:49537-49548.
- Doyle DA, Morais CJ, Pfuetzner RA, Kuo A, Gulbis JM, Cohen SL, Chait BT, and MacKinnon R (1998) The structure of the potassium channel: molecular basis of K<sup>+</sup> conduction and selectivity. *Science* **280**:69-77.

- Fedida D, Eldstrom J, Hesketh JC, Lamorgese M, Castel L, Steele DF, and Van Wagoner DR (2003) Kv1.5 is an important component of repolarizing K<sup>+</sup> current in canine atrial myocytes. *Circ Res* **93**:744-751.
- Feng J, Wible B, Li GR, Wang Z, and Nattel S (1997) Antisense oligodeoxynucleotides directed against Kv1.5 mRNA specifically inhibit ultrarapid delayed rectifier K<sup>+</sup> current in cultured adult human atrial myocytes. *Circ Res* **80**:572-579.
- Fernandez D, Ghanta A, Kauffman GW, and Sanguinetti MC (2004) Physicochemical features of the HERG channel drug binding site. *J Biol Chem* **279**:10120-10127.
- Franqueza L, Longobardo M, Vicente J, Delpon E, Tamkun MM, Tamargo J, Snyders DJ, and Valenzuela C (1997) Molecular determinants of stereoselective bupivacaine block of hKv1.5 channels. *Circ Res* **81**:1053-1064.
- Han W, Wang Z, and Nattel S (2000) A comparison of transient outward currents in canine cardiac Purkinje cells and ventricular myocytes. *Am J Physiol (Heart Circ Physiol)* **279**:H466-H474.
- Herrera D, Yue L, Wang Z, and Nattel S (2002) Effects of antiarrhythmic drugs on currents carried by dKv3.1 and hKv1.5. *Biophys J* **82**:585a. Abstract
- Hockerman GH, Johnson BD, Abbott MR, Scheuer T, and Catterall WA (1997). Molecular determinants of high affinity phenylalkylamine block of L- type calcium channels in transmembrane segment IIS6 and the pore region of the alpha1 subunit. *J Biol Chem* **272**:18759-18765.
- Hughey R and Krogh A (1996) Hidden Markov models for sequence analysis: extension and analysis of the basic method. *Comput Appl Biosci* **12**:95-107.
- Jiang Y, Lee A, Chen J, Cadene M, Chait BT, and MacKinnon R (2002) The open pore conformation of potassium channels. *Nature* **417**:523-526.

- Judge SI, Yeh JZ, Goolsby JE, Monteiro MJ, and Bever CT Jr (2002) Determinants of 4-aminopyridine sensitivity in a human brain Kv1.4 K(+) channel: phenylalanine substitutions in leucine heptad repeat region stabilize channel closed state. *Mol Pharmacol* **61**:913-920.
- Laskowski BR, MacArthur MW, Moss DS, and Thornton JM (1993) PROCHECK: A program to check the stereochemical quality of protein structures. *J Appl Cryst* **26**:283-291.
- Lees-Miller JP, Duan Y, Teng GQ, and Duff HJ (2000) Molecular determinant of high-affinity dofetilide binding to HERG1 expressed in *Xenopus* oocytes: involvement of S6 sites. *Mol Pharmacol* **57**:367-374.
- Liu Y, Holmgren M, Jurman ME, and Yellen G (1997) Gated access to the pore of a voltage-dependent K<sup>+</sup> channel. *Neuron* **19**:175-184.
- Mitcheson JS, Chen J, Lin M, Culberson C, and Sanguinetti MC (2000) A structural basis for drug-induced long QT syndrome. *Proc Natl Acad Sci U S A* **97**:12329-12333.
- Nattel S, Khairy P, Roy D, Thibault B, Guerra P, Talajic M, and Dubuc M (2002) New approaches to atrial fibrillation management: a critical review of a rapidly evolving field. *Drugs* **62**:2377-2397.
- Nattel S, Yue L, and Wang Z (1999) Cardiac ultrarapid delayed rectifiers, a novel potassium current family of functional similarity and molecular diversity. *Cell Physiol Biochem* **9**:217-226.
- Perry M, de Groot MJ, Helliwell R, Leishman D, Tristani-Firouzi M, Sanguinetti MC, and Mitcheson J (2004) Structural determinants of HERG channel block by clofilium and ibutilide. *Mol Pharmacol* **66**:240-249.

- Ragsdale DS, McPhee JC, Scheuer T, and Catterall WA (1996) Common molecular determinants of local anesthetic, antiarrhythmic, and anticonvulsant block of voltage-gated  $\text{Na}^+$  channels. *Proc Natl Acad Sci U S A* **93**:9270-9275.
- Roden DM and George AL Jr (1997) Structure and function of cardiac sodium and potassium channels. *Am J Physiol* **273**:H511-H525.
- Sali A and Blundell TL (1993) Comparative protein modelling by satisfaction of spatial restraints. *J Mol Biol* **234**:779-815.
- Seeböhm G, Chen J, Strutz N, Culberson C, Lerche C, and Sanguinetti MC (2003) Molecular determinants of KCNQ1 channel block by a benzodiazepine. *Mol Pharmacol* **64**:70-77.
- Snyders DJ (1999) Structure and function of cardiac potassium channels. *Cardiovasc Res* **42**:377-390.
- Sunami A, Dudley SC Jr, and Fozzard HA (1997) Sodium channel selectivity filter regulates antiarrhythmic drug binding. *Proc Natl Acad Sci U S A* **94**:14126-14131.
- Tamargo J, Caballero R, Gomez R, Valenzuela C, and Delpon E (2004) Pharmacology of cardiac potassium channels. *Cardiovasc Res* **62**:9-33.
- Varro A, Biliczki P, Iost N, Virag L, Hala O, Kovacs P, Matyus P, and Papp JG (2004). Theoretical possibilities for the development of novel antiarrhythmic drugs. *Curr Med Chem* **11**:1-11.
- Wang S, Morales MJ, Qu YJ, Bett GC, Strauss HC, and Rasmusson RL (2003) Kv1.4 channel block by quinidine: evidence for a drug-induced allosteric effect. *J Physiol* **546**:387-401.
- Wang Z, Fermini B, and Nattel S (1995) Effects of flecainide, quinidine, and 4-aminopyridine on transient outward and ultrarapid delayed rectifier currents in human atrial myocytes. *J Pharmacol Exp Ther* **272**:184-196.

- Wang Z, Fermini B, and Nattel S (1993) Sustained depolarization-induced outward current in human atrial myocytes. Evidence for a novel delayed rectifier  $K^+$  current similar to Kv1.5 cloned channel currents. *Circ Res* **73**:1061-1076.
- Wang Z, Pagé P, and Nattel S (1992) Mechanism of flecainide's antiarrhythmic action in experimental atrial fibrillation. *Circ Res* **71**:271-287.
- Weerapura M, Nattel S, Chartier D, Caballero R, and Hébert TE (2002) A comparison of currents carried by HERG, with and without coexpression of MiRP1, and the native rapid delayed rectifier current. Is MiRP1 the missing link? *J Physiol (Lond)* **540**:15-27.
- Weiner SJ, Kollman PA, Case DA, Singh UC, Ghio C, Alagona G, Profeta S, and Weiner P (1984) A new force field for molecular mechanical simulation of nucleic acids and proteins. *J Amer Chem Soc* **106**:765-784
- Wulff H, Gutman GA, Cahalan MD, and Chandy KG (2001) Delineation of the clotimazol/TRAM-34 binding site on the intermediate conductance calcium activated potassium channel, IKCa1. *J Biol Chem* **276**:30240-30245.
- Yamagishi T, Ishii K, and Taira N (1995) Antiarrhythmic and bradycardic drugs inhibit currents of cloned  $K^+$  channels, Kv1.2 and Kv1.4. *Eur J Pharmacol* **281**:151-159.
- Yeola SW, Rich TC, Uebele VN, Tamkun MM, and Snyders DJ (1996) Molecular analysis of a binding site for quinidine in a human cardiac delayed rectifier  $K^+$  channel. Role of S6 in antiarrhythmic drug binding. *Circ Res* **78**:1105-1114.
- Yeola SW and Snyders DJ (1997) Electrophysiological and pharmacological correspondence between Kv4.2 current and rat cardiac transient outward current. *Cardiovasc Res* **33**:540-547.
- Yue L, Feng J, Li GR, and Nattel S (1996) Characterization of an ultrarapid delayed rectifier potassium channel involved in canine atrial repolarization. *J Physiol (Lond)* **496**:647-662.

- Yue L, Wang Z, Rindt H, and Nattel S (2000a) Molecular evidence for a role of Shaw (Kv3) potassium channel subunits in potassium currents of dog atrium. *J Physiol* **527**:467-478.
- Yue L, Feng JL, Wang Z, and Nattel S (2000b) Effects of ambasilide, quinidine, flecainide and verapamil on ultra-rapid delayed rectifier potassium currents in canine atrial myocytes. *Cardiovasc Res* **46**:151-161.
- Zhang H, Zhu B, Yao JA, and Tseng GN (1998) Differential effects of S6 mutations on binding of quinidine and 4-aminopyridine to rat isoform of Kv1.4: common site but different factors in determining blockers' binding affinity. *J Pharmacol Exp Ther* **287**:332-343.
- Zhang S, Zhou Z, Gong Q, Makielski JC, and January CT (1999) Mechanism of block and identification of the verapamil binding domain to HERG potassium channels. *Circ Res* **84**:989-998.

## Footnotes

<sup>1</sup> This work was supported by the Canadian Institutes of Health Research, the Quebec Heart and Stroke Foundation and the Mathematics of Information Technology and Complex Systems (MITACS) Network.

<sup>2</sup> Reprint requests: Dr Stanley Nattel, Research Center, Montreal Heart Institute, 5000 Belanger St E, Montreal, Quebec, Canada, H1T 1C8. Tel.: (514)-376-3330; Fax: (514)-376-1355; E-mail: stanley.nattel@icm-mhi.org

## FIGURE LEGENDS

**Figure 1.** Flecainide inhibition of Kv3.1 and Kv1.5 currents expressed in *Xenopus* oocytes ( $n=8$  per observation). Kv3.1 (**A**) and Kv1.5 (**C**) currents induced by depolarization to potentials ranging from -50 mV to +60 mV from a holding potential of -60 mV in the absence and presence of 50  $\mu$ M flecainide. Inset shows the voltage-clamp protocol used to elicit currents. Vertical scales represent 1  $\mu$ A and horizontal scales 100 ms. Current-voltage relationships for Kv3.1 (**B**) and Kv1.5 (**D**) currents in the absence ( $\circ$ ) and presence of 50  $\mu$ M flecainide ( $\square$ ) (\*\*  $P<0.01$ , \*\*\*  $P<0.001$  versus control).

**Figure 2.** **A**, effects of four concentrations of flecainide on currents recorded in representative oocytes expressing Kv3.1 and Kv1.5 (protocol in inset). Note that all recordings before and after drug were in the same oocyte. Vertical scales represent 1  $\mu$ A and horizontal scales 100 ms. **B**, concentration-response curves for Kv3.1 and Kv1.5 (mean $\pm$ S.E.M.) for effects of flecainide upon steps to +30 mV ( $n=8$  per observation). **C**, percentage reduction (mean $\pm$ S.E.M.) in Kv3.1 and Kv1.5 as a function of test potential at 50 and 500  $\mu$ M flecainide. **D**, **E**, activation voltage-dependence of Kv3.1 and Kv1.5 currents under control conditions and in the presence of 50 and 500  $\mu$ M flecainide respectively, as determined based on the tail current at -30 mV following steps to each of the voltages indicated normalized to the tail current after a step to +60 mV ( $n=8$  per observation).

**Figure 3.** Time-dependent flecainide effects. **A**, **B**, mean $\pm$ S.E.M. blocking rate constants (determined as illustrated in insets) were a linear function of flecainide concentration ( $n=8$  oocytes/data point). Insets: fractional inhibition of Kv3.1 (**A**)

and Kv1.5 (**B**) current produced by the flecainide concentration indicated relative to control (given by  $[(I_{\text{Ctl}} - I_{\text{Flec}})/I_{\text{Ctl}}]$ ) are shown as a function of time during voltage steps to +30 mV. Original data are shown, as well as best-fit exponentials to determine the rate constants for block onset. **C**, **D**, tail currents were elicited upon repolarisation to -30 mV following pulses to +60 mV from a holding potential of -60 mV. Kv3.1 (**C**) and Kv1.5 (**D**) deactivation currents (tail currents) in the absence and presence of the indicated flecainide concentration. **E**, summary data (mean $\pm$ SEM) of time course of deactivation in the absence and presence of flecainide concentrations indicated in panels **C** and **D** (results were obtained in 8 oocytes per construct).

**Figure 4.** Effects of flecainide on currents carried by WT and chimeric subunits. **A**, current recordings in absence and presence of 50  $\mu$ M flecainide. **B**, concentration-response curves for Kv3.1 WT, Kv3.1 with the Kv1.5 S6 and C-terminal (Kv3.1/Kv1.5 S6+C-term), Kv1.5 WT and Kv1.5 with the Kv3.1 S6 and C-terminal (Kv1.5/Kv3.1 S6+C-term). **C**,  $IC_{50}$ s for flecainide effects on currents upon application of a pulse to +30 mV. (\* $P < 0.05$  versus Kv3.1 WT;  $\dagger\dagger P < 0.01$  versus Kv1.5 WT, N ranges from 6 to 8). Vertical calibrations are 1  $\mu$ A and horizontal calibrations are 100 ms. (Kv3.1/1.5C-term=chimera formed by substituting Kv1.5 C-terminal into Kv3.1; Kv1.5/3.1C-term=chimera formed by substituting Kv3.1 C-terminal into Kv1.5).

**Figure 5.** Amino-acid sequence comparison of the region between the beginning of the S5-S6 linker and S6 in dKv3.1, hKv1.5, rKv4.2 and rKv1.4. Residues selected for mutation analysis are boxed.

**Figure 6.** *A*, effects of four concentrations of flecainide on currents recorded in representative oocytes expressing WT and various mutant constructs of Kv3.1 (left) and Kv1.5 (right) (voltage protocol in inset). Vertical calibrations are 1  $\mu$ A and horizontal calibrations are 100 ms. *B*, mean $\pm$ S.E.M. IC<sub>50</sub>s for WT and mutant constructs (\**P*<0.05, \*\*\**P*<0.001 versus Kv1.5WT; †*P*<0.05, †††*P*<0.001 versus Kv3.1 WT, n ranges from 6 to 8 per data point). *C*, concentration-response curves for WT and isoleucine/leucine mutants mean $\pm$ S.E.M. for effects of flecainide upon steps to +30 mV (n ranges from 6 to 8 per data point).

**Figure 7.** Effects of flecainide on I<sub>o</sub>-forming subunits. *A*, current recordings of Kv4.2 WT, Kv4.2 L492I, Kv1.4 WT and Kv1.4 I547L in the absence (left panels) and presence (right panels) of 50  $\mu$ M flecainide (recordings before and after drug were always obtained in the same oocyte). *B*, concentration-response curves for flecainide inhibition of currents elicited by depolarization to +30 mV. Vertical calibrations are 1  $\mu$ A and horizontal calibrations are 100 ms.

**Figure 8.** Homology model of the Kv3.1 pore. Structural model of the Kv3.1 pore region obtained by homology modeling using the MthK crystal structure as template (PDB: 1LNQ). Top and side views of the predicted Kv3.1 channel S5-Pore-S6 region shown in a ribbon representation. The channel selectivity filter is illustrated containing two K<sup>+</sup> ions (orange). The L422 (red) and the cavity lining residue V425 (yellow) are represented as van der Waals surfaces. Only three of the four monomers have been included in the side view representation of the channel for clarity. This model predicts that the L422 residue is positioned behind V425. As a result L422 is not expected to face the channel central cavity and thus to interact directly with flecainide. The position of the hydrophilic L401 and I389 residues has

been marked in green and blue respectively. The I389 residue is predicted to be located in the N-terminal end of the channel pore helix (blue) whereas the L401 residue is seen as part of the selectivity filter. Mutation of these residues is not expected to affect the structure of the channel central cavity where most likely binding of flecainide takes place.

TABLE 1  
 Primers used for chimera and point mutation construction

Clone	Primers and Annealing Temperatures in °C	RES
<b>Kv3.1 I389D</b>	1. CTGCCCAACAAGATAGAGTTCAT } 2. CAGAAGCCATCGGGGATGTTCTTAAAGTGGG } 3. GTCATGGTGACCACGGCCCACCAGAAGCCATCGGGGA } } 57 } } 55	<i>MscI</i> <i>BstEII</i>
<b>Kv1.5 D469I</b>	1. AGCGGGTTCATGGCCCCGCCCTCT } 2. ACCAGAAGGCGATAGGGATGCTAG } 3. CATGGTGACCACTGCCACCAGAAGGCGATAGGGATGC } } 60 } } 59	<i>PmlI</i> <i>BstEII</i>
<b>Kv3.1 L401V</b>	1. ATGACGACGGTGGGCTACGGAGAC } 2. GCCCGTGGTACCATGACGACGGTGGGCTAC } 3. ATCGGATCCTCAAGTCACTCTCAC } } 54 } } 54	<i>BstEII</i> <i>BamHI</i>
<b>Kv1.5 V481L</b>	1. AGTGGTCACCATGACCACTCTGGGCTACGGGGA } 2. CATGATATCTCACAATCTGTTTCCCGGCT } } 58	<i>BstEII</i> <i>EcoRV</i>
<b>Kv3.1 L422I</b>	1. GCACTGTGTGCGATAGCGGGCGTGCTG } 2. ATCGGATCCTCAAGTCACTCTCAC } } 53	<i>BstAPI</i> <i>BamHI</i>
<b>Kv1.5 I502L</b>	1. TCCAGTGCCGTCTACTTCGCA } 2. AGGACCCCGCGAGGGCACACAGCGAG } 3. GCTGTGTGCCCTCGCCGGGTCCTCAC } 4. CATGATATCTCACAATCTGTTTCCCGGCT } } 57 } } 57 } } 59	<i>BstEII</i> <i>EcoRV</i>
<b>Kv4.2 L392I</b>	1. GCCCCTGGTGTCTACTATGT } 2. GACCAAGACTCCGCTAATTGAGCAGAT } 3. GGGTCTATCTGCTCAATTAGCGGAGTC } 4. ATAGTTTAGCGGCCGCTTACAAAGCAGACAC } } 53 } } 49 } } 54	<i>BsmBI</i> <i>NotI</i>
<b>Kv1.4 I547L</b>	1. GCAGAGGCAGATGAACCTACC } 2. TAAGACACCCGCAAGGGCACACAG } 3. GGGTCCCTGTGTGCCCTTGCGGGTGTG } 4. GATGGATCCTCAGACGTCAGTCTC } } 53 } } 52 } } 54	<i>BsmI</i> <i>BamHI</i>
<b>Kv3.1/ Kv1.5S6- Cterm</b>	1. CAAGATAAGCTTATGGGCCAAGGGGACGAGAGCGAG } 2. CCCGGCGATGGCACACAGCGAGCCCACGATCATGCCG } GACCACGTCTGCGGGTA } 3. GACATGTACCCGCAGACGTGGTCCGGCATGATCGTGG } GCTCGCTGTGTGCCATC } 4. ACGAATGAGCTCTCACAATCTGTTTCCCGGCTGGT } } 63 } } 63 } } 61	<i>HindIII</i> <i>SacI</i>
<b>Kv1.5/ Kv3.1S6- Cterm</b>	1. CAAGATAAGCTTATGGAGATCGCCCTGGTGGCCCTG } 2. GCCCGCCAGCGCACACAGTGCTCCACCAGCTTGCC } CCCAACAGTGATGGGCT } 3. GACATGAGGCCCATCACTGTTGGGGGCAAGCTGGTG } GGAGCACTGTGTGCGCTG } 4. ACGAATGGATCCTCAAGTCACTCTCACAGCCTCTGT } } 63 } } 61 } } 59	<i>HindIII</i> <i>BamHI</i>
<b>Kv3.1/ Kv1.5Cterm</b>	1. ATAGGGGCCCAGCCCAATGAC } 2. CACGATGACGGGCACAGGCAT } 3. GTTGAAGTTGGACACGATGACGGG } 4. TCCAACCTCACTACTTCTACCACCGG } 5. ACGAATGAGCTCTCACAATCTGTTTCCCGGCTGGT } 6. CCCGTCATCGTCCAACCTCACTACTTCTAC } } 59 } } 49 } } 59 } } 53 } } 54	<i>BstEII</i> <i>SacI</i>
<b>Kv1.5/ Kv3.1Cterm</b>	1. TCCAGTGCCGTCTACTTCGCA } 2. GACGATGACGGGCACAGGCAG } 3. CCCAAAATTGTTGACGATGACGGG } 4. AACAAATTTGGGATGTATTACTCC } 5. ACGAATGGATCCTCAAGTCACTCTCACAGCCTCTGT } 6. CCCGTCATCGTCAACAATTTTGGGATGTATTACTCC } } 57 } } 48 } } 54 } } 54 } } 55	<i>BstEII</i> <i>BamHI</i>

RES: Restriction Endonuclease Sites

TABLE 2

Rate constants for wild-type and mutant channels.

Channel	$k_{\text{on}}(\mu\text{M}^{-1}\text{s}^{-1})$	$k_{\text{off}}(\text{s}^{-1})$	$K_{\text{d}}(\mu\text{M})$
Kv3.1 WT	1.4±0.1	39.8±5.3	28.8±3.6
Kv3.1 L422I	0.37±0.05	73.2±4.5	202.7±11.7
Kv1.5 WT	0.30±0.02	60.0±5.5	210.8±5.9
Kv1.5 I502L	1.1±0.3	36.7±1.6	35.4±1.9

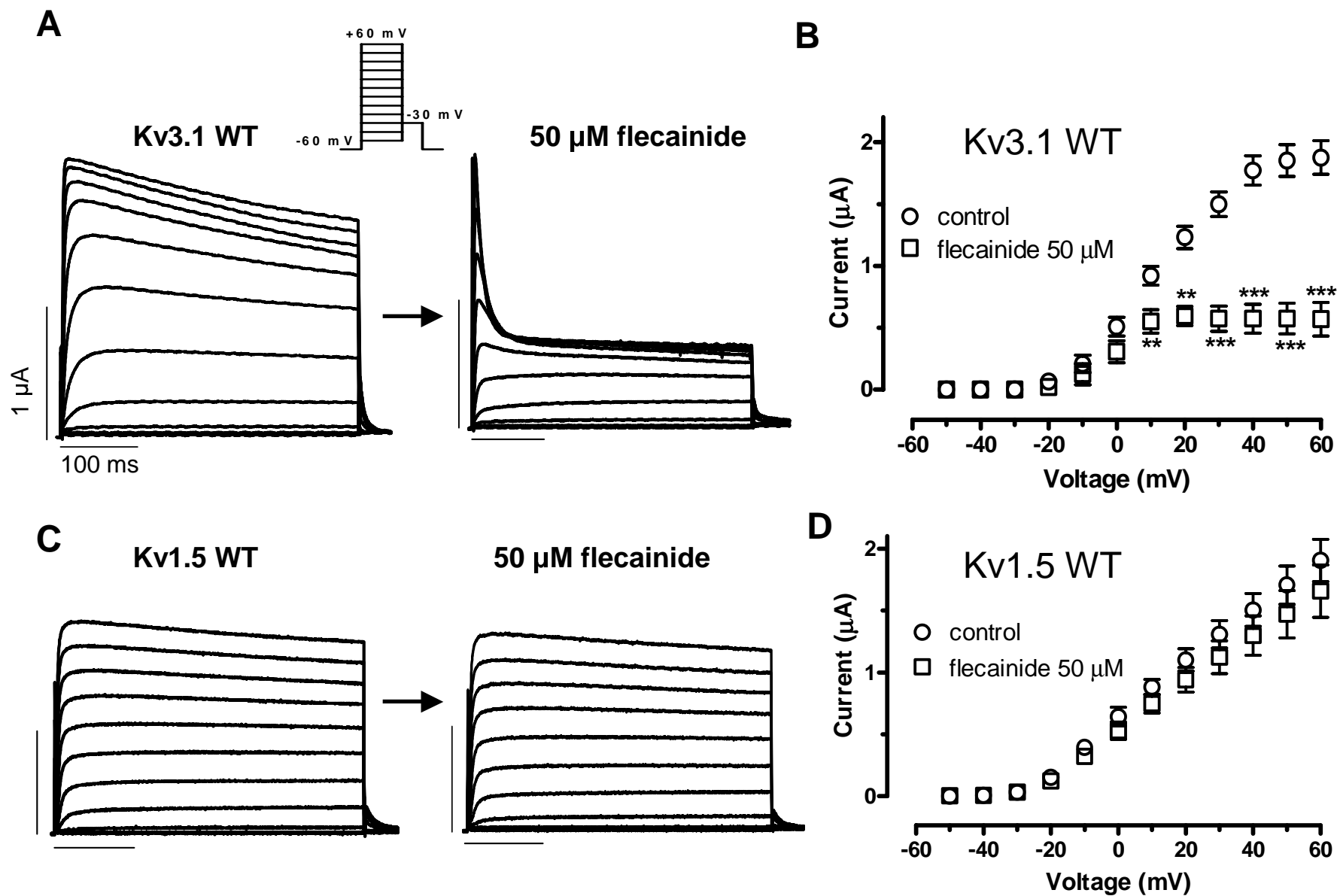
TABLE 3

Biophysical properties of wild-type and mutant clones

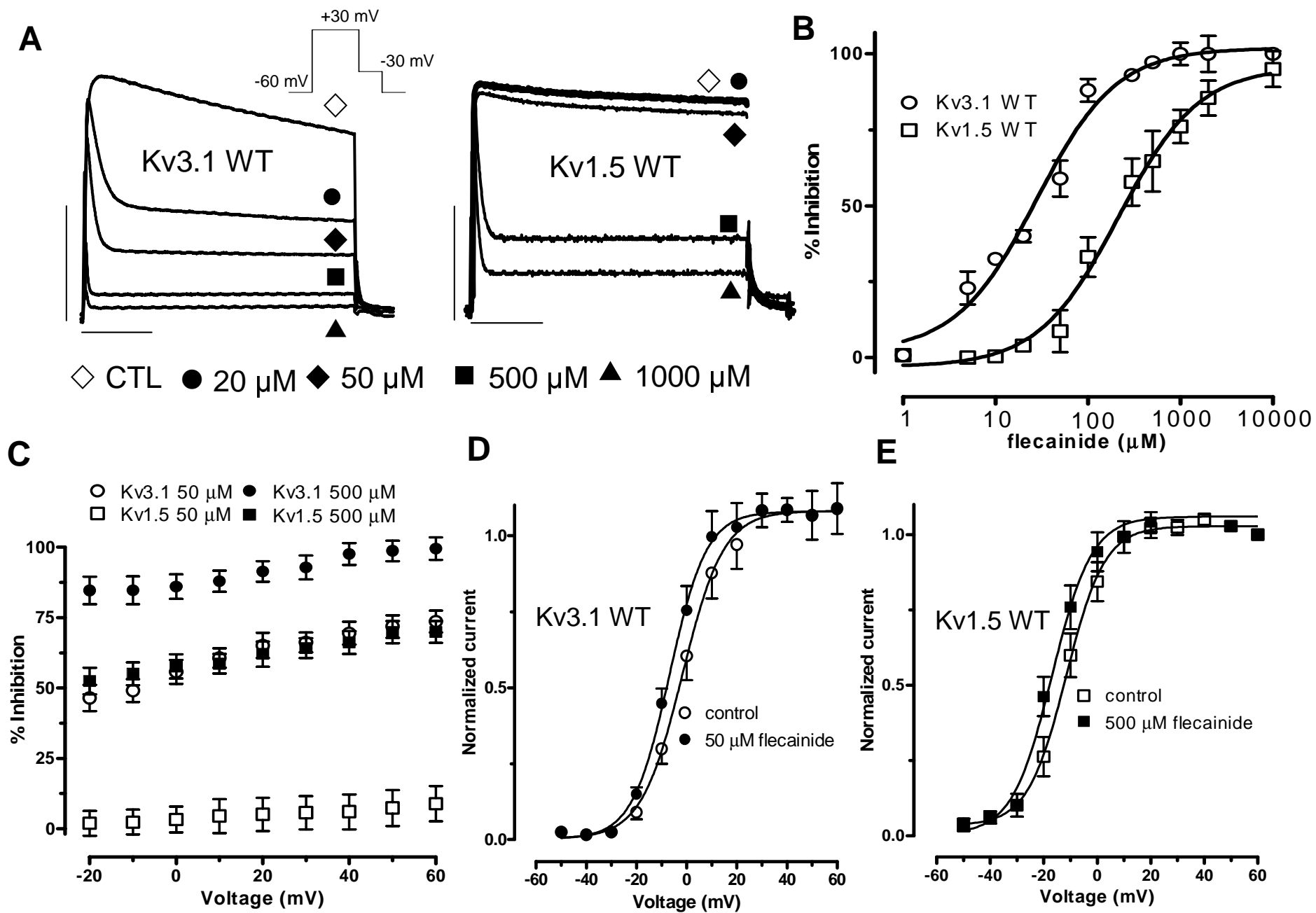
Clone	$V_{1/2}$ (mV)	$k$ (mV)	$\tau_{-10\text{mV}}$ (ms)	$\tau_{+30\text{mV}}$ (ms)	$V_{\text{rev}}$ (mV)
Kv3.1 WT	-1.7±0.4	8.2±1.1	19.4±1.5	3.9±0.5	-78±3.2
Kv3.1 L422I	-2.1±0.5	8.0±1.5	18.7±1.9	3.5±0.9	-76±4.8
Kv1.5 WT	-11.6±1.8	7.2±1.2	9.8±1.1	2.7±0.3	-73±3.4
Kv1.5 I502L	-10.3±1.7	7.0±1.4	9.6±1.6	2.5±0.6	-74±4.6

$V_{1/2}$  = 50% activation voltage;  $k$  = slope factor of activation curve;  $\tau_{-10\text{mV}}$ ,  $\tau_{+30\text{mV}}$  = activation time constants at -10 and +30 mV respectively,  $V_{\text{rev}}$  = reversal potential based on reversal of tail currents following a 25 ms activating pulse to +30 mV.

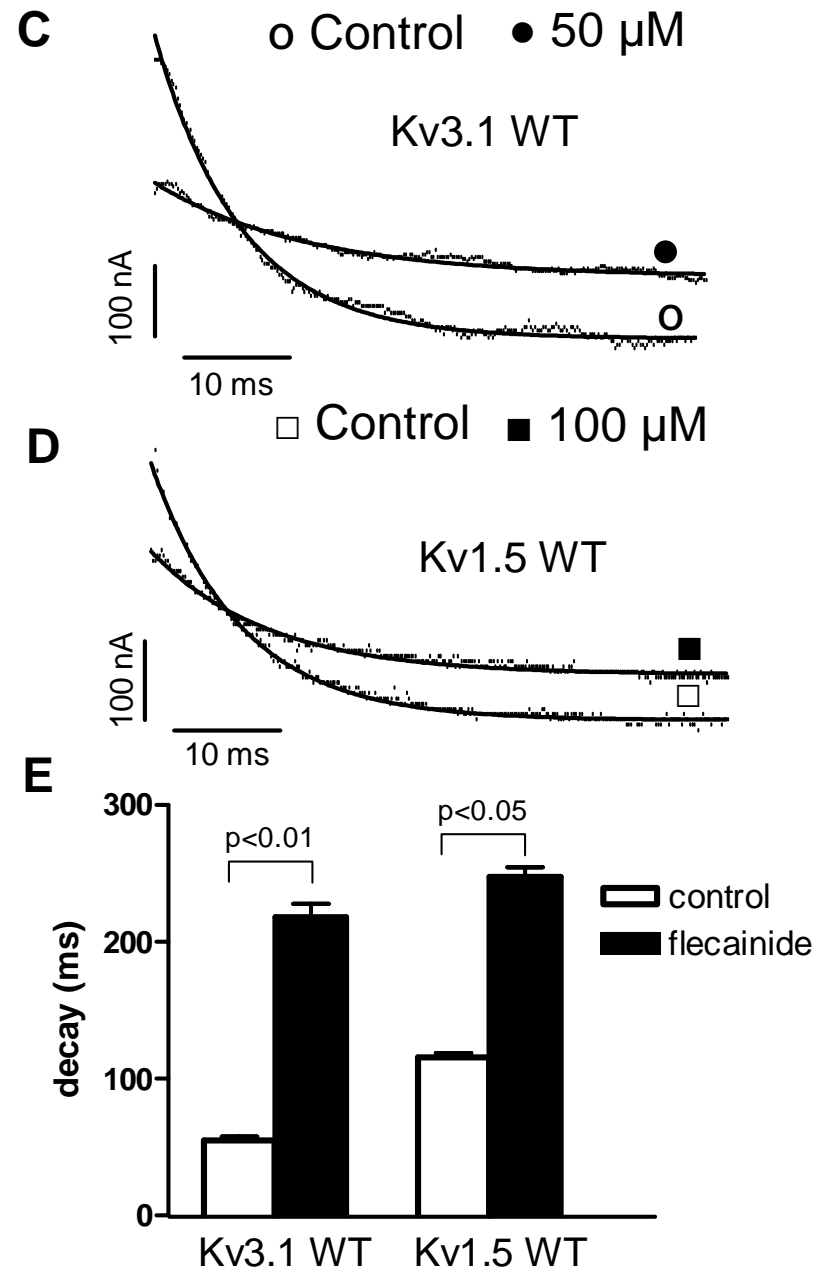
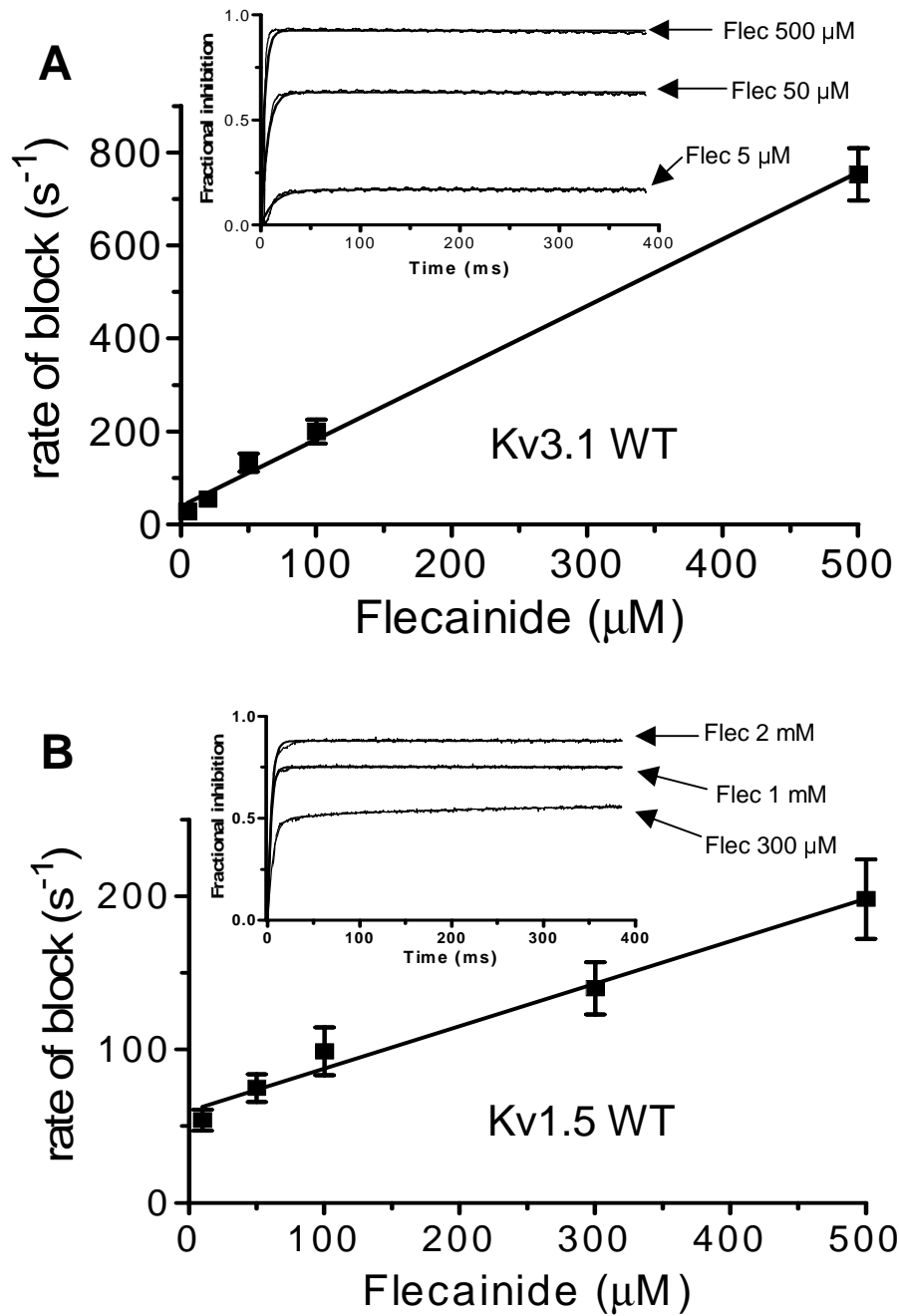
Figure 1



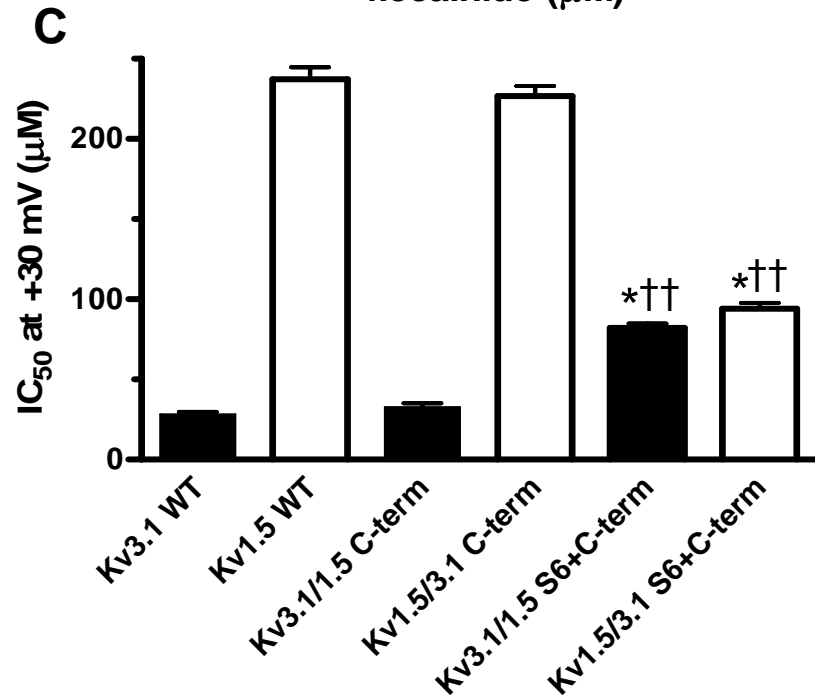
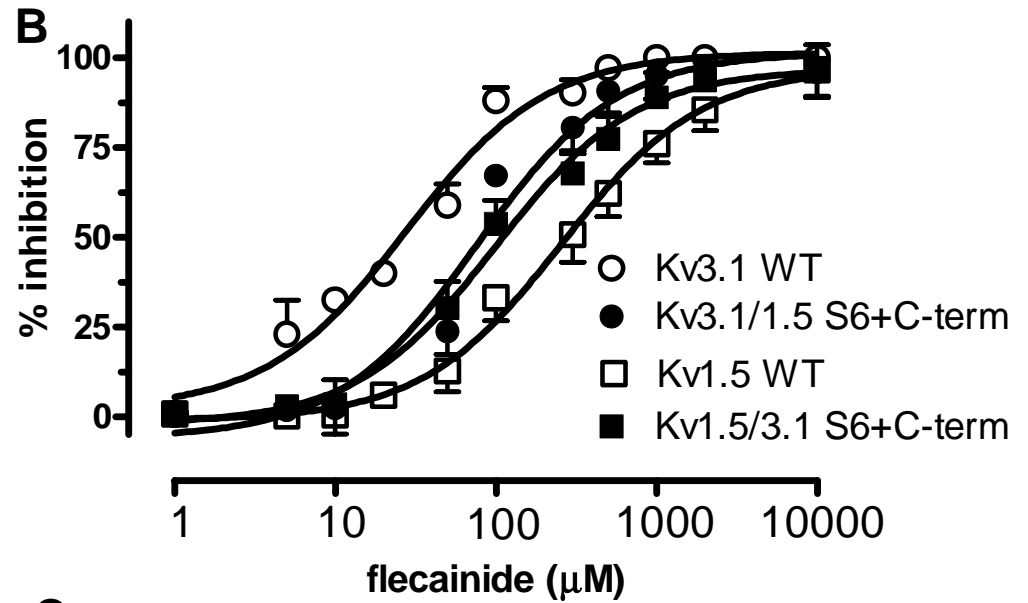
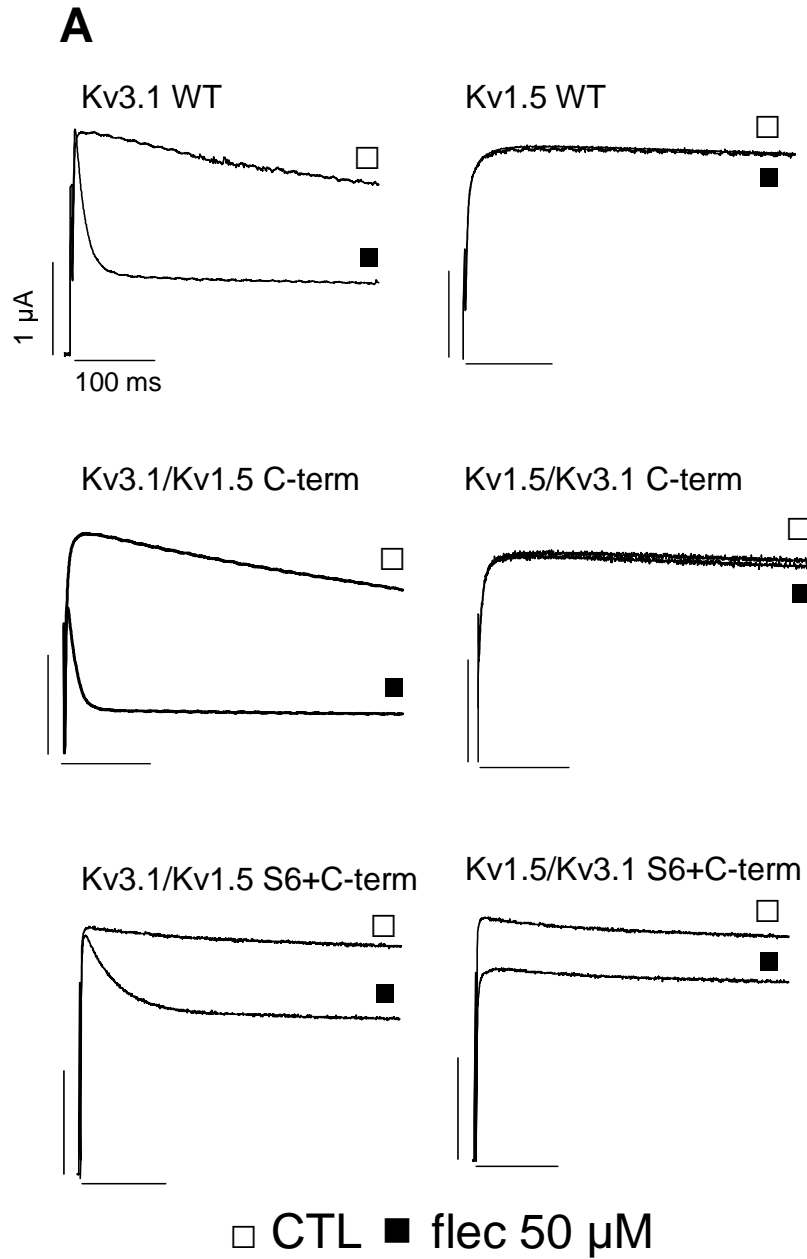
**Figure 2**



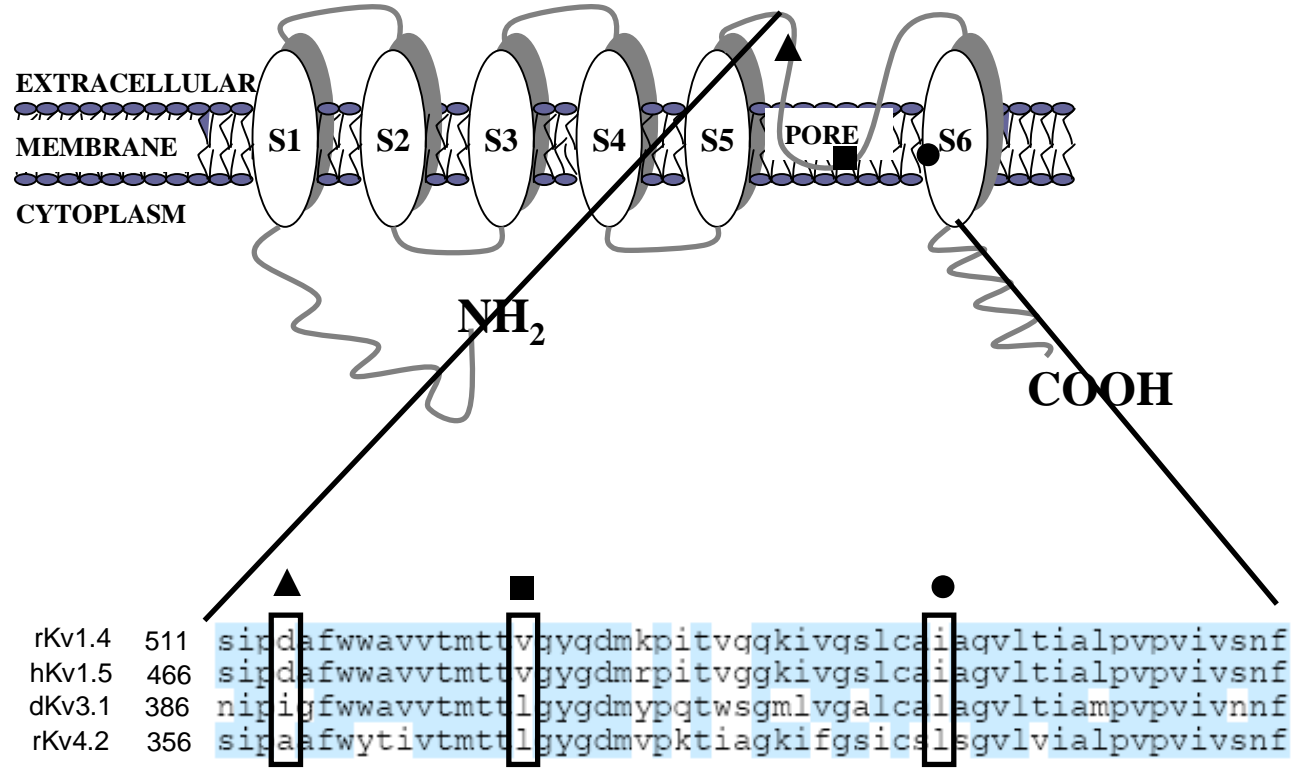
**Figure 3**



**Figure 4**



**Figure 5**



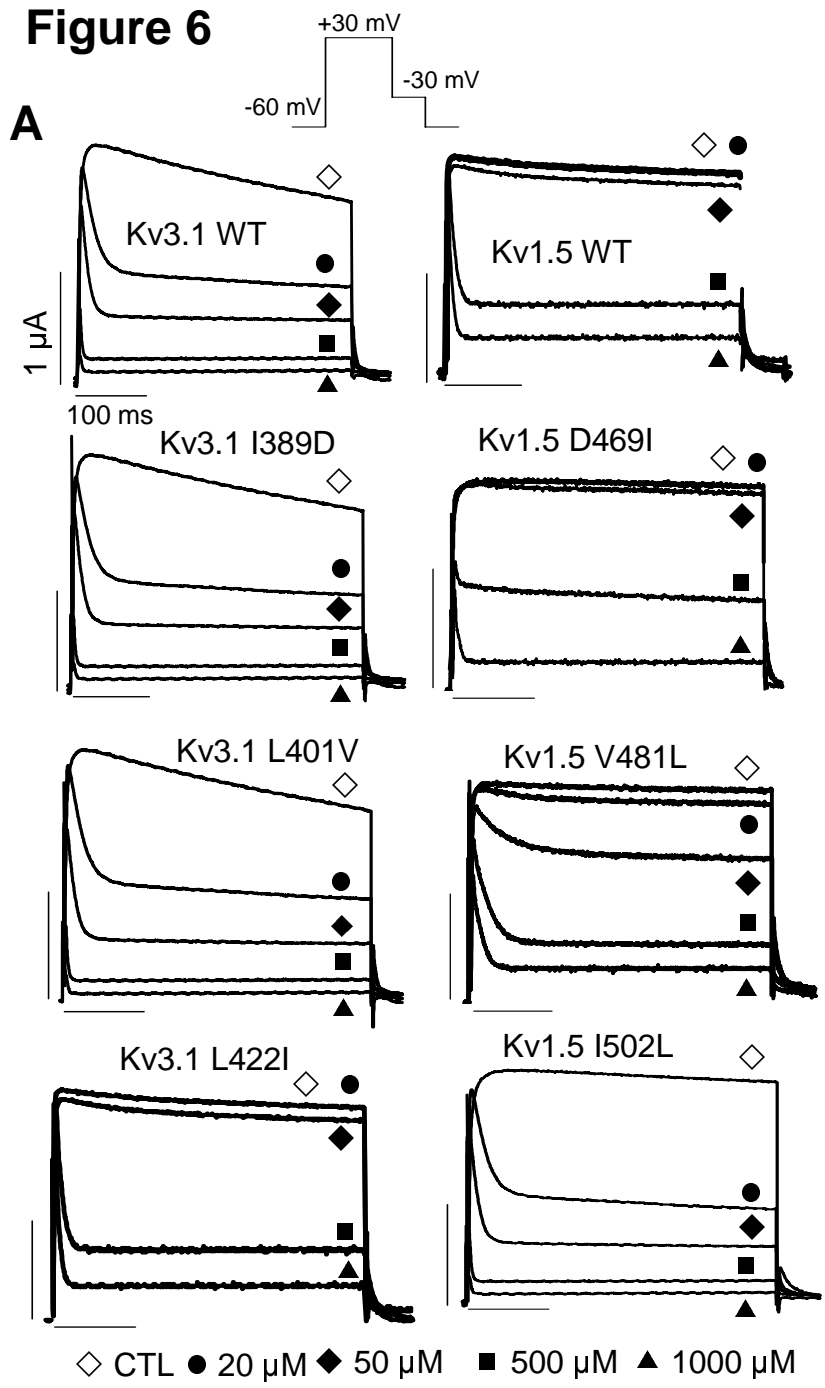


**Figure 7**

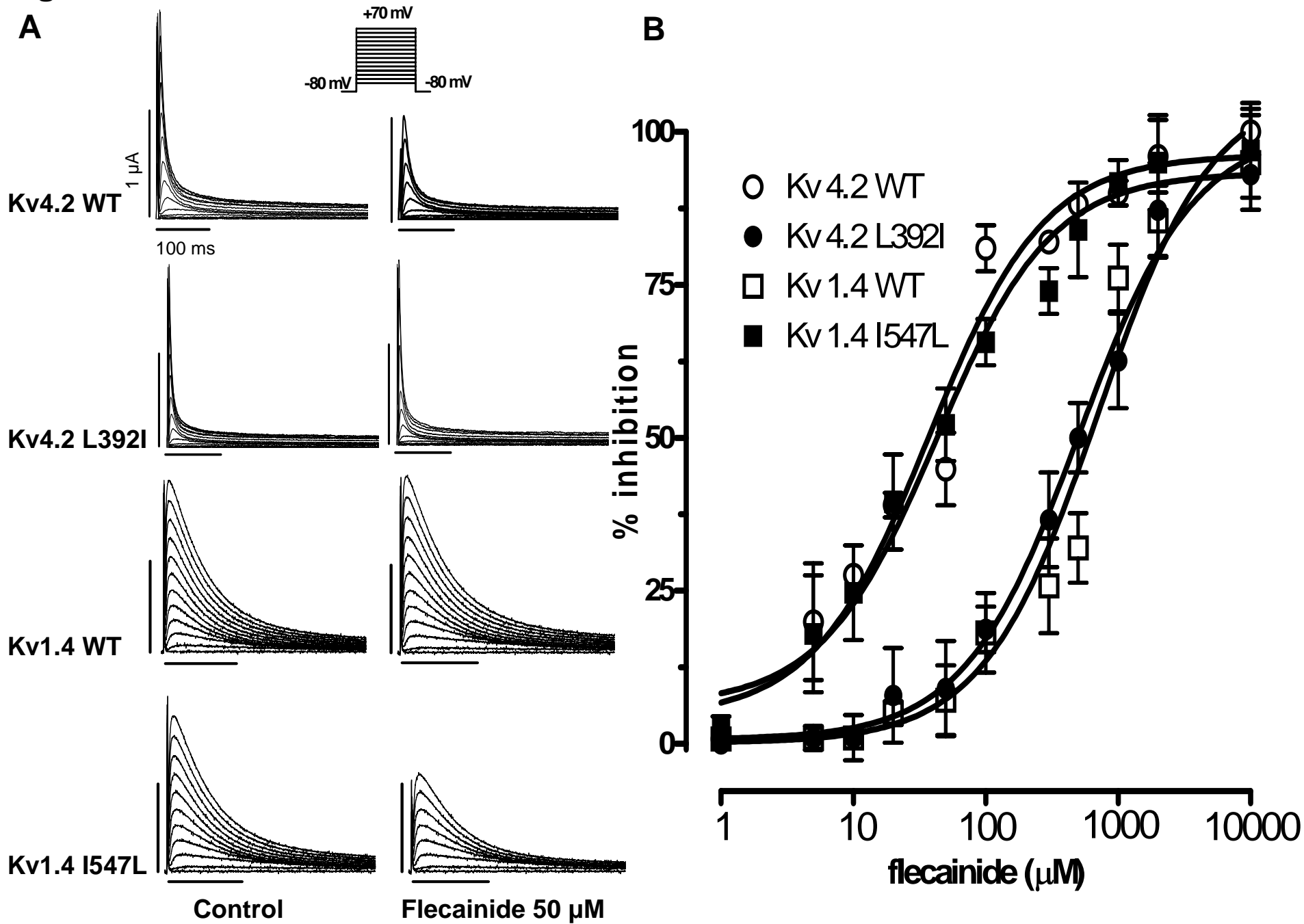


Figure 8

